9 (2): 241-248 (2025)

Journal of Aviation

https://dergipark.org.tr/en/pub/jav

e-ISSN 2587-1676

A Comparative Metamodel Based Shape Optimization Study for Maximizing Thrust of a Helicopter Rotor Blade Under a Torque Constraint

Emin Burak Özyılmaz[1], Mustafa Kaya[2*]

[1]Ankara Yıldırım Beyazıt University, Aerospace Engineering Department, 06020, Ankara, Türkiye. (eminburakozyilmaz@aybu.edu.tr)
[2*] Ankara Yıldırım Beyazıt University, Aerospace Engineering Department, 06020, Ankara, Türkiye. (mkaya@aybu.edu.tr)

Article Info

Received: 03 January 2025
Revised: 27 March 2025
Accepted: 14 May 2025
Published Online: 22 June 2025

Keywords:
Machine Learning
Optimization
Aerodynamics
CFD

Corresponding Author: *Mustafa Kaya*

RESEARCH ARTICLE

https://doi.org/10.30518/jav.1612888

Abstract

The solution of Reynolds-Averaged Navier-Stokes (RANS) equations is crucial for accurately predicting the aerodynamic loads on helicopter rotor blades. In particular, the computational process required for blade shape optimization, involving numerous RANS solutions, is highly time-consuming. To reduce this computational cost, a recently adopted approach is the use of metamodels, such as machine learning methods. A well-established metamodel is expected to successfully replicate CFD solutions. In this study, different machine learning techniques were employed as metamodels and evaluated based on a series of CFD solutions. The machine learning models aimed to capture the functional relationship between the generated thrust and torque and the twist distribution along the rotor blade. The smooth twist variation was modelled using a 3-knot cubic spline, with five parameters serving as inputs for the spline definition. The optimal twist distribution was determined concerning a reference helicopter rotor blade, the Caradonna-Tung rotor blade. The optimization scenarios were defined to maximize thrust force while maintaining the baseline torque value. The optimal cases were identified using the Quadratic Response Surface Method, Support Vector Regression, and Artificial Neural Network Regression. As a result of this study, a significant increase in the thrust force generated by the helicopter rotor blade was observed.

1. Introduction

Computational Fluid Dynamics (CFD) is a widely used tool to analyze and improve the aerodynamical performance of designs in industries such as aerospace, automotive and energy. In aerospace engineering point of view, wings, rotors and bodies need to be designed as efficiently as possible. However, it is a challenging task to produce an optimized solution when it comes to helicopter rotor blades since the helicopter rotor blades are operating in unsteady and vortical regimes (Vu & Lee, 2015) and multidisciplinary influences such as aerodynamics, flight mechanics, dynamics etc. (Conlisk, 1997; Newman, 2007; You & Jung, 2017). Many researchers (Celi, 1999; Ganguli, 2004) studied on rotor blade aerodynamic shape optimization to improve the efficiency of the blades.

Sun and Lee (H. Sun & Lee, 2005) conducted an optimization study on Caradonna-Tung helicopter rotor blade. They investigated the shape of a rotor blade using 3D CFD and numerical optimization methodology such as response surface method. Airfoil design and blade tip shape have been studied under subsonic and transonic flow regimes in hovering condition.

McVeigh and McHugh (McVeigh & McHugh, 1984) conducted a study to investigate the effects of different tip shapes, chord lengths, blade numbers and different airfoils on rotor blade performances. They conducted several wind tunnel tests. The efficiency of hover condition influenced by the airfoil section, taper of tip location and number of blades.

Costes et al. (Costes et al., 2012) studied on CFD techniques developed at ONERA for helicopter blades. They stated that helicopter rotor blade simulations are complex due to multidisciplinary conditions around the helicopter such that aerodynamics, aeroelastics and flight dynamics strongly interact with each other. They gave an overview of CFD methodologies to solve highly unsteady flows with shockwaves, separated flows and vortices.

Wang and Zhao (Wang & Zhao, 2020) studied on a new rotor blade shape. The parameters were twist distribution, chord length variation and sweep. They used CFD techniques and an optimization methodology. As a result of that study, a better lift to drag ratio, an increased coefficient of thrust at the same coefficient of torque and increased Figure of Merit have been achieved with the new airfoil design.

Haider et al. (Haider et al., 2017) used response surface methodology to optimize an unmanned agricultural helicopter rotor blade hover efficiency. The rotor has been improved by several percentages in both thrust and torque.

Machine Learning methods have been effectively used in aerospace industries to find solutions to some problems by learning from an appropriate dataset (Bishop, 2006). Well trained machine learning methods with sufficient dataset may be accurate for predicting solutions (Li et al., 2022). Once a set of CFD based flow solutions have been obtained in terms of the given values of a number of design variables, a machine learning model may be trained to obtain the flow solutions for the other values of design variables (Kaya, 2019).

Glaz et al. (Glaz et al., 2008) studied on surrogate based optimization method to reduce the helicopter rotor vibration. They compared the accuracies of kriging, radial basis functions and polynomial regression methods. The results are compared to a baseline blade and it is seen that surrogate based optimization can effectively be done in helicopter rotor blade studies. Giunta et al.(Giunta et al., 1995) presented a design methodology for High Speed Civil Transport aircraft wings. They focused on applying Response Surface Methodology to design steps. The objective function of the optimization is to minimize the gross take-off weight of an aircraft in the boundaries of the design space.

In the last decade, machine learning techniques have been integrated into optimization procedures to make the search for optimized aerodynamic shapes easier and more cost-effective by generating metadata from experimental or numerical results (Renzoni et al., 2000). Sun et al.(G. Sun et al., 2015) studied to find the optimized shape of an airfoil or a wing by using Artificial Neural Networks in an inverse design methodology. They stated that their design procedure which contains a properly trained neural network and a database of airfoils or wings improved the design efficiency. Andres Perez et al.(Andrés-Pérez et al., 2019) presented a 36 geometric design variable optimization study on a common model wing DPW-W1 by using Support Vector Machines as metamodel. They stated that a single point-constrained optimization procedure shows promising results on a three-dimensional wing in both viscous and inviscid flows. Li and Zhang (Li & Zhang, 2021) studied on to present a data-based approach for geometric optimization of a wing in transonic conditions. Their database consists of more than 135000 data samples. The features of database have different wing shapes and flight conditions. Deep Neural Networks have been used to determine the optimum values of aerodynamic coefficients of a wing with a very small error. Zhang et al.(Zhang et al., 2021) presented an effective shape optimization method based on deep neural networks. The database is constructed with CFD computations which solved both fine and coarse grids. They stated that the method had been proposed is an efficient and effective method for both airfoils and wing design frameworks. An extensive literature review (Li et al., 2022) can be seen to examine the subject in more detail.

The aim of this study is to compare different metamodel performances to find the optimized geometric shape of a helicopter rotor blade that maximizes the thrust force produced by the rotor blade while not producing more torque than the basic geometry. This approach will create an innovative and comprehensive framework to address one of the most complex and critical challenges in helicopter rotor design which is blade optimization. By combining advanced and novel methodologies such as Computational Fluid Dynamics and machine learning methods, the proposed framework seeks to boost design efficiency, enhance aerodynamic performance, and play a key role in shaping the next generation of rotorcraft technologies. Geometric shape optimization consists of only a smooth twist distribution which is defined by a three knot cubic spline along the span. Quadratic Response Surface Method, Support Vector Regression and Artificial Neural Network modelling have been used as metamodels. The data for training these metamodels have been generated from three dimensional CFD solutions of different cases which are recommended by a design of experiment method. The results of the optimization procedure compared to each other and a new blade shape recommended.

2. Materials and Methods

The method used in helicopter rotor blade optimization is given as a process flow chart in Figure 1. In this study, the process starts with the validation of the numerical method and continues with the generation of the data set. In the flow diagram, training of machine learning algorithms and performing optimization studies are the other sequential steps in the process.

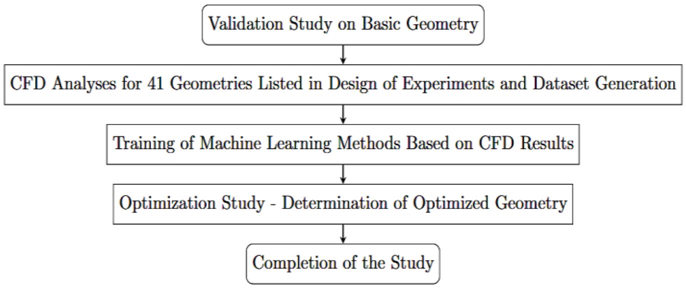

Figure 1. Process flow chart of this paper

The Caradonna–Tung helicopter rotor blade (Caradonna & Tung, 1981) has been selected as the base rotor blade for the optimization study. A three-dimensional Reynolds Average Navier Stokes solver is used to calculate the flow around the rotor blades. The shape of the rotor blade is defined by changing the twist distribution along the blade. The twist angles are changed along the blade using a cubic spline method, which changes the twist angles corresponding to the root, middle and tip positions of the rotor blade. The Box-Behnken design of experiment method (Box & Behnken, 1960) is applied to efficiently manage the selection of numerical analyses to be performed, and thus a number of samples are generated.

2.1. Caradonna-Tung Helicopter Rotor Blade

The Caradonna-Tung helicopter rotor consists of two untwisted and untapered blades. NACA0012 airfoil is used from root to tip. The rotor has a radius of 1.143 m, with a constant chord length of 0.1905 m along the span. The blade's taper stacking point, or taper axis, is located at 25% of the chord length from the leading edge. For the numerical analysis in this study, the blades are connected to the hub through a circular section. The airfoil begins transitioning at 10% of the blade span radially from the rotor's center of rotation. The sectional twist center is defined at 25% of the chord length from the leading edge for the twist distribution. A schematic representation of the rotor blade is given in Figure 2.

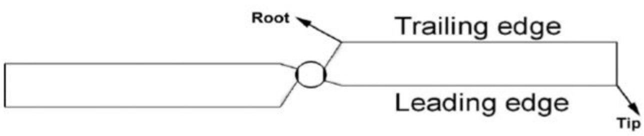

Figure 2. Front view of Caradonna-Tung rotor blade

2.2. Flow Domain

The flowfields has been computed with FINE/Turbo CFD software which is a 3-dimensional, compressible, structured, multi-block finite volume solver. It is a specially developed software to compute both internal and external flows for turbomachinery with a capability of preconditioning for low Mach number flows.

O4H grid strategy has been used to generate mesh around the blades with IGG/AutoGrid5. A schematic representation of the 5-block mesh is provided in Figure 3 with following components:

1) an O block around the blade

2) a H block upstream the leading edge of the blade

3) a H block downstream the trailing edge

4) a H block up to the blade section

5) a H block down to the blade section

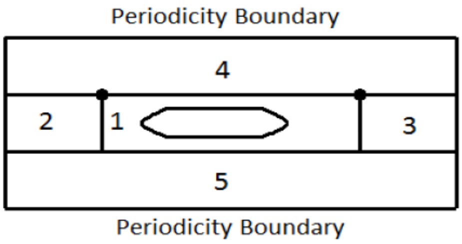

Figure 3. O4H Grid Strategy for mesh generation

Solid boundaries have been modelled as no-slip walls which enforces the fluid velocity to have the same velocity with the rotating surfaces. On the farfield boundaries the flow variables are determined by Riemann invariants. The angular velocity is set to 1750 RPM. It should be noted that all computations have been done at hover condition which means that there is no freestream velocity. Since the Caradonna-Tung helicopter rotor blade is symmetric, only one portion of the domain has been generated. Farfield and periodic boundary conditions can be seen in Figure 4.

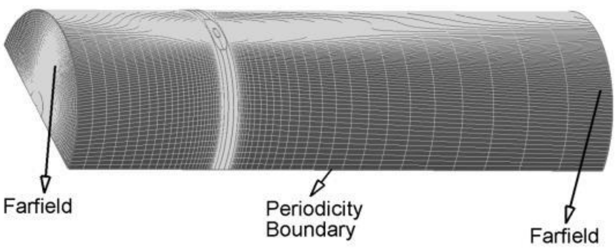

Figure 4. Boundary conditions for flow domain

2.3. Twist Distribution with Cubic Splines

A cubic spline is one of type of splines which is built with piecewise third order polynomials which passes through a set of knots. First and second derivatives are continuous at each knot which provides smoothness of the data. Additionally, constructing a cubic spline requires knowledge of the first derivatives at the endpoints.

In this study, 3 knots (r_{root}, r_{mid} and r_{tip}) have been used to construct the cubic spline with 3 corresponding twist angle values ($\theta_{root}, \theta_{mid}$ and θ_{tip}). The first derivative at the first knot, that is, $\left.\frac{d\theta}{dr}\right|_{root}$ and the first derivative at the third knot, that is, $\left.\frac{d\theta}{dr}\right|_{tip}$ are included.

A mathematically expressed summary of the cubic spline used to define the spanwise twist distribution, $\theta = \theta(r)$ is given in Equation 1:

$$\begin{gathered} if\ r_{root} \le r \le r_{mid} \\ \theta_1(r) = a_1(r - r_{root})^3 + b_1(r - r_{root})^2 + c_1(r - r_{root}) + d_1 \\ if\ r_{mid} \le r \le r_{tip} \\ \theta_2(r) = a_2(r - r_{root})^3 + b_2(r - r_{root})^2 + c_2(r - r_{root}) + d_2 \end{gathered} \tag{1}$$

where the unknown coefficients, $a_1, b_1, c_1, d_1, a_2, b_2, c_2$ and d_2 are determined according to the following conditions:

Equation 1 leads to a linear system for 8 unknowns, which is easily solved.

$$\begin{aligned} \theta_1(r_{root}) &= \theta_{root} \\ \theta_1(r_{mid}) &= \theta_{mid} \\ \theta_2(r_{mid}) &= \theta_{mid} \\ \theta_2(r_{tip}) &= \theta_{tip} \\ \left.\frac{d\theta_1}{dr}\right|_{mid} &= \left.\frac{d\theta_2}{dr}\right|_{mid} \\ \left.\frac{d^2\theta_1}{dr^2}\right|_{mid} &= \left.\frac{d^2\theta_2}{dr^2}\right|_{mid} \\ \left.\frac{d\theta_1}{dr}\right|_{root} &= \left.\frac{d\theta}{dr}\right|_{root} \\ \left.\frac{d\theta_2}{dr}\right|_{tip} &= \left.\frac{d\theta}{dr}\right|_{tip} \end{aligned} \tag{2}$$

2.4. Design of Experiment

Design of Experiment (DOE) refers to the methodologies employed to effectively organize and select the experiments to be conducted (Cavazzuti, 2013). These methods facilitate the systematic planning, design, and analysis of experiments (Antony, 2014). In this study, the dataset is generated utilizing the Box-Behnken Design of Experiment methodology.

The cubic spline for smooth twist variation along the span is defined by five parameters which are $\left(\boldsymbol{\theta_{root}}, \boldsymbol{\theta_{mid}}, \boldsymbol{\theta_{tip}}, \left.\frac{d\theta}{dr}\right|_{root} \textbf{ and } \left.\frac{d\theta}{dr}\right|_{tip}\right)$. For a 5-element input vector, the Box-Behnken method recommends 41 input-output pairs.

Table 1 provides the minimum, maximum, and intermediate values for this DOE.

Table 1. Input values for Box-Behnken DoE

Variable	Parameter	Min	Int	Max
$\vec{x}_1$	θ_{root}	-5.0	5.0	15.0
$\vec{x}_2$	θ_{mid}	-5.0	5.0	15.0
$\vec{x}_3$	θ_{tip}	-5.0	5.0	15.0
$\vec{x}_4$	$\left.\frac{d\theta}{dr}\right\|_{root}$	-15.0	0.0	15.0
$\vec{x}_5$	$\left.\frac{d\theta}{dr}\right\|_{tip}$	-15.0	0.0	15.0

The rotor blade geometry is defined by 26 cross-sections, spanning from the root to the tip. Figure 5 depicts the twist angles along the blade span, as derived from the Design of Experiment (DoE). Notably, the convex hull of the DoE serves as the feasible domain for determining the optimal twist distribution.

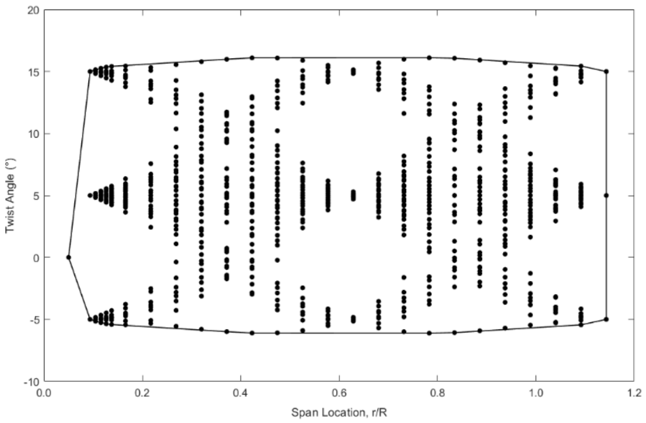

Figure 5. Feasible domain for optimum twist distribution along blade

2.5. Machine Learning Methods

In this study, machine learning techniques were employed to develop metamodels tailored to the dataset and to represent the dataset as a functional relationship. The methods utilized include Quadratic Response Surface Method (QRSM), Support Vector Regression (SVR), and Artificial Neural Networks (ANN) regression. The regression models were implemented in Python using the Scikit-Learn library.

2.5.1. Quadratic Response Surface Method (QRSM)

Response Surface Methodology (RSM) is a statistical and mathematical approach commonly applied to model and analyze problems where a response variable is affected by multiple factors, aiming to optimize the response(H. Sun & Lee, 2005). Experimental data are utilized to build an approximate model of the response. Among the various models in RSM, the second-order polynomial equation which is also known as quadratic, as shown in Equation 3, is the most frequently used.

$$y = \beta_0 + \sum_{i=1}^{k} \beta_i x_i + \sum_{i=1}^{k} \beta_{ii} x_i^2 + \sum_{i<j} \beta_{ij} x_i x_j \qquad (3)$$

where

y: Predicted response

β_0: Intercept term

$\beta_i, \beta_{ii}, \beta_{ij}$: Coefficients of linear, quadratic, and interaction terms, respectively

x_i, x_j: Input variables

2.5.2. Support Vector Regression (SVR)

Support Vector Regression (SVR) is a robust machine learning method based on the principles of Support Vector Machines (SVM). Although SVM is primarily intended for classification tasks, SVR adapts these principles for regression, allowing the prediction of continuous target variables. The fundamental concept of SVR is to identify a function that maps input features to the target variable, while simultaneously minimizing prediction error and controlling model complexity (Li et al., 2022).

The general form of SVR to approximate the $\boldsymbol{y} = \boldsymbol{y}(\vec{\boldsymbol{x}})$ is expressed as follows:

$$y^*(\vec{x}) = \langle \vec{w}, \vec{\emptyset}(\vec{x}) \rangle + b \qquad (4)$$

where $\langle \cdot \ , \ \cdot \rangle$ denotes the dot product, $\vec{x}$ is the vector of input variables, y^* is an approximation function to the target function y, $\vec{w}$ is the weight vector, $\vec{\emptyset}$ is a vector valued function of $\vec{x}$ and b is a constant. In the literature, $\vec{\emptyset}$ and b are respectively called as the (non-linear) feature mapping function and the bias.

There are two aims while building the SVR model. The first aim is to determine the approximation function, $y^*(\vec{x})$ which has at most ε deviation from the actual target, $y(\vec{x})$. The second aim is to make $y^*(\vec{x})$ as flat as possible.

Therefore, the following optimization problem is solved:

$$\begin{gathered} \underset{\vec{w}, \xi_i^+, \xi_i^-}{minimize} \quad \frac{1}{2}\left|\left|\vec{w}\right|\right|^2 + C\sum_{i=1}^{m}(\xi_i^+ + \xi_i^-) \\ \text{Subject to} \\ \langle \vec{w}, \vec{\emptyset}(\vec{x}_i) \rangle + b - y_i \leq \varepsilon + \xi_i^+ \\ y_i - \langle \vec{w}, \vec{\emptyset}(\vec{x}_i) \rangle - b \leq \varepsilon + \xi_i^- \\ \xi_i^+, \xi_i^- \geq 0 \ i = 1,2,,,,m \end{gathered} \qquad (5)$$

where $\vec{x}_i$ and y_i denote the i^{th} input-output pair in the training data set. m, is the number of data pairs in the entire set or in a subset of the entire set, depending on the training algorithm. ε, is called the loss function and is a model parameter that must be supplied before solving the minimization problem in Equation 5. The penalty parameter, C > 0, is also a model parameter and must be supplied a priori as well. It determines the trade-off between the flatness of $y^*(\vec{x})$ and the amount up to which deviations larger than ε are tolerated. Finally, ξ_i^+, ξ_i^- are called as the slack variables which provide a feasible solution to Equation 4 in the feasible domain by copying with the ε constraint.

2.5.3. Artificial Neural Network

Artificial Neural Networks (ANNs) are the cornerstone of deep learning, renowned for their scalability and robustness, making them ideal for tackling large-scale and complex machine learning problems.

The architecture of an ANN consists of three main components: an input layer, one or more hidden layers, and an output layer. The input layer represents the input parameters, while the output layer corresponds to the target quantities to be predicted. Each layer is composed of multiple neurons, and within each neuron, the following operation takes place:

In an artificial neural network, the operation within a single neuron is defined in Equation 6:

$$z = \sum_{i=1}^{n} \vec{w}_i \vec{x}_i + b \qquad (6)$$

where:

$\vec{x}$ is the input vector,

$\vec{w}$ is the vector of weights to be learned,

b is the bias term,

z is the output of the neuron, which serves as input for the next layer.

The result z is then passed through an activation function, such as ReLU, sigmoid, or tanh, to introduce non-linearity, enabling the network to learn complex relationships in the data.

Commonly used activation functions include the sigmoid, hyperbolic tangent, and ReLU functions.

The sigmoid activation function is expressed in Equation 7:

$$\sigma(z) = \frac{1}{1 + e^{-z}}, \quad (7)$$

where:

z is the input to the function, typically a weighted sum of neuron inputs plus a bias term.

The sigmoid activation function is monotonic and differentiable, with outputs in the range $[0,1]$. However, its derivative is non-monotonic.

Another commonly used activation function is the hyperbolic tangent function, given in Equation 8:

$$\tanh(z) = \frac{e^{z} - e^{-z}}{e^{z} + e^{-z}}. \quad (8)$$

The hyperbolic tangent function outputs values in the range $[-1,1]$, providing a broader range of nonlinearity compared to the sigmoid function.

The ReLU (Rectified Linear Unit) activation function is defined as follows:

$$f(x) = \begin{cases} x, & x > 0 \\ 0, & x \leq 0 \end{cases} \quad (9)$$

where:

x is the input to the function, typically the weighted sum of neuron inputs plus a bias term. ReLU introduces non-linearity into the model while maintaining computational efficiency, as it simply outputs the input directly if it is positive and outputs zero otherwise. This simplicity makes it computationally faster compared to other activation functions.

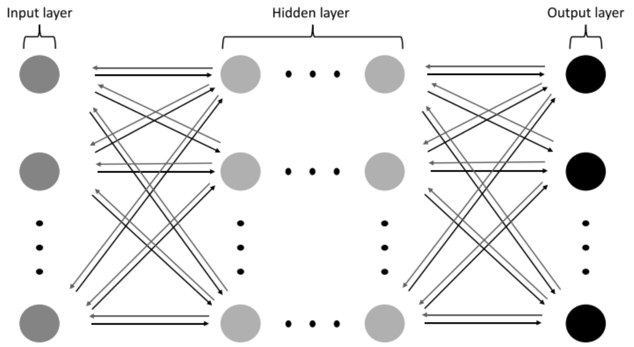

Figure 6. A Schematic representation of Artificial Neural Networks(Li et al., 2022)

2.6. Evaluation Metrics

The performance of regression models can be evaluated using various metrics, such as Mean Absolute Error (MAE), Root Mean Square Error (RMSE), and the Coefficient of Determination (R^2).

2.6.1. Mean Absolute Error (MAE)

MAE measures the average absolute difference between observed and predicted values for continuous variables.

$$\text{MAE} = \frac{1}{n}\sum_{i=1}^{n} |y_i - \hat{y}_i| \quad (10)$$

where:

n: Number of observations,

y_i: Observed values,

$\hat{y}_i$: Predicted values.

Equation 10 provides a straightforward interpretation of the average magnitude of errors in the predictions, without considering their direction (positive or negative). A smaller MAE indicates better predictive accuracy.

2.6.2. Root Mean Square Error (RMSE)

RMSE measures the square root of the average squared differences between observed and predicted values.

$$\text{RMSE} = \sqrt{\frac{1}{n}\sum_{i=1}^{n} (y_i - \hat{y}_i)^2} \quad (11)$$

where:

n: Number of observations,

y_i: Observed values,

$\hat{y}_i$: Predicted values.

Equation 11 gives higher weight to large errors due to the squaring operation, making it sensitive to outliers. A smaller RMSE indicates a better fit of the regression model.

2.6.3. Coefficient of Determination (R^2)

The R^2 value is a statistical measure that indicates how well the regression model explains the variability in the dataset. It is computed using Equation 12:

$$R^2 = 1 - \frac{\sum (y_i - \hat{y}_i)^2}{\sum (y_i - \bar{y})^2} \quad (12)$$

where:

y_i: Observed values,

$\hat{y}_i$: Predicted values.

$\bar{y}$: Mean of the observed values.

The R^2 value ranges between 0 and 1, where 1 indicates that the model explains all the variability in the data, and 0 indicates no explanatory power. A higher R^2 value signifies a better fit of the model to the data.

2.7. Optimization

In this study, the design vector, $\vec{x}$, is represented by the cubic spline parameters, while the objective functions are defined as the required torque, $y_1(\vec{x})$, and the produced thrust, $y_2(\vec{x})$, have been given in Equation 13.

$$\vec{x} = \begin{bmatrix} x^{(1)} \\ x^{(2)} \\ x^{(3)} \\ x^{(4)} \\ x^{(5)} \end{bmatrix} = \begin{bmatrix} \theta_{root} \\ \theta_{mid} \\ \theta_{tip} \\ d\theta/dr|_{root} \\ d\theta/dr|_{tip} \end{bmatrix} \quad (13)$$

$$y_1^*(\vec{x}) = required\ torque$$
$$y_2^*(\vec{x}) = produced\ thrust$$

Once a metamodel is developed, an analytical fitting function is established to map the input to the output. The extremum of this analytical function can be readily determined by setting its first derivative to zero, as there are no constraints on the twist parameters.

$$\frac{dy^*(\vec{x})}{dx} = 0 \tag{14}$$

The optimization problem is given Equation 15, where a represents the maximum allowable torque specified by the user. $\overrightarrow{lb}$ and $\overrightarrow{ub}$ correspond to the lower and upper bounds of the cubic spline parameters. As the system of equations in Equation 14 is non-linear, it requires a numerical solution. In this study, the solution is obtained iteratively using Newton's method.

$$\begin{gathered} maximize\ y_2(\vec{x}), \vec{x} \in R^n \\ \text{Subject to} \\ y_1(\vec{x}) \leq a \\ \overrightarrow{lb} \leq \vec{x} \leq \overrightarrow{ub} \end{gathered} \tag{15}$$

3. Results and Discussion

3.1. Validation Study

The CFD software FINE/Turbo has been benchmarked against the results of the Caradonna-Tung experiment. The flow domain was constructed using approximately 7 million elements, with the first layer thickness near the solid boundaries set to $3 \times 10^{-6} m$, ensuring a y^+ value close to 1.

Spalart-Allmaras turbulence model has been implied and the Reynolds number is about 4×10^6.

Table 2 provides the experimental torque and thrust values, alongside a comparison with the CFD results. The CFD computations were conducted to evaluate the performance of the Caradonna-Tung Rotor Blade under the same operating conditions. The results demonstrate a strong correlation between the experimental data and the numerical predictions.

Table 2. Experiment compared to CFD

	Torque	Thrust
Experiment	135 Nm	1150 N
CFD	136 Nm	1149 N
Error (%)	0.7	0.1

3.2. Generation of Dataset

According to the Box-Behnken design of experiment methodology, appropriate geometric configurations were generated, and three-dimensional CFD simulations were conducted to determine the thrust force and the required torque values.

Table 3. Ten Different samples of the Dataset

$\vec{x}_1$	$\vec{x}_2$	$\vec{x}_3$	$\vec{x}_4$	$\vec{x}_5$	Produced Thrust (N)	Required Torque (Nm)
0	5	-5	-5	0	2233	321
0	5	5	-5	15	1371	211
0	5	-5	5	15	1323	152
0	15	5	-5	0	1241	198
15	5	5	-5	0	1227	186
0	15	-5	5	0	1205	144
15	5	-5	5	0	1204	138
0	-5	-5	5	0	1204	134
-15	5	5	-5	0	1189	179
-15	5	-5	5	0	1188	135
0	-5	5	-5	0	1160	172

Steady-state flow solutions were obtained using local time stepping in each cell. Table 3 presents ten different samples from the dataset, which actually contains 41 cases.

3.3. Evaluation Metrics

In this study, the results of different machine learning techniques were analyzed based on evaluation metrics defined in Section 2.6. All three methods were assessed in terms of MAE, RMSE, and $\boldsymbol{R^2}$, and the results are presented in Tables 4 and 5 below.

In QRSM and SVR methods, a separate training process is performed for each output variable. This is because these methods produce scalar values as output rather than vectors. However, in ANN, outputs can be treated as a vector, allowing a single training process to generate a metamodel for datasets with multiple outputs. While Table 4 presents the evaluation results of the machine learning methods for the Produced Thrust output, $y_1(\vec{x})$, Table 5 provides the evaluation results for the Required Torque output, $y_2(\vec{x})$. It should be noted that, since ANN undergoes a single training process, the evaluation metrics remain the same for both output variables.

Table 4. Evaluation Metrics for Produced Thrust Output

	MAE	RMSE	R^2
QRSM	1.07E-12	1.52E-12	1
SVR	1.86667472	2.387305	0.999974
ANN	0.267760486	0.346905	0.999973

According to the evaluation metrics, QRSM appears to have demonstrated the best performance, delivering near-perfect results. In particular, the MAE and RMSE values being close to zero highlight the model's exceptionally low prediction errors. It should be noted that such highly scored training data results raise a suspicion of overfitting.

Table 5. Evaluation Metrics for Required Torque Output

	MAE	RMSE	R^2
QRSM	6.11E-14	9.37E-14	1
SVR	0.719088968	0.888885	0.99972
ANN	0.267760486	0.346905	0.999973

ANN, while showing slightly higher errors compared to QRSM, achieved significantly better accuracy than SVR. The RMSE and MAE values of ANN are considerably lower than those of SVR.

SVR exhibited the highest error values among the three models but still demonstrated strong compatibility with the data, as indicated by its relatively high R-squared value.

3.4. Optimization Results

The optimization study was conducted using metamodels developed with QRSM, SVR, and ANN Regression. The optimized results were identified within the feasibility region defined by Equation 15, where a represents the baseline torque, set to 135 Nm. The lower and upper bounds in Equation 15 correspond to the minimum and maximum values derived from the design of experiment.

As a result of the optimization studies, the optimal rotor blade configurations were determined for each model. These configurations were optimized to achieve the maximum possible thrust force without exceeding the torque value of the baseline geometry. Table 6 presents the blade shapes in terms of the design variables.

Table 6. Optimum cases for corresponding methods

Model Name	$\left.\frac{d\theta}{dr}\right\|_{root}$	θ_{root}	θ_{mid}	θ_{tip}	$\left.\frac{d\theta}{dr}\right\|_{tip}$
QRSM	-5.318	-5	-5	6.551	15
SVR	5.136	-3.286	-3.651	2.764	-2.884
ANN	5.78	-5	-3.38	1.84	-0.132

Figure 7 shows the spanwise twist distributions of the blades which are recommended by models.

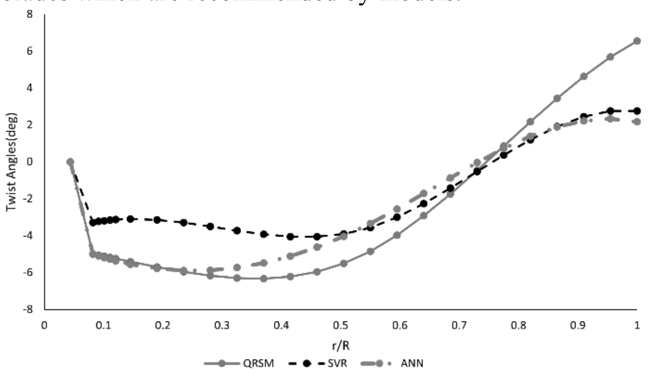

Figure 7. Spanwise twist distributions of optimum cases

The predictions from the optimization study were validated against CFD simulations. Table 7 provides a comparison between the model predictions and the CFD results for the optimal twist distributions. It was observed that there are some deviations in the predictions of the QRSM and SVR models. However, the thrust predicted by the Artificial Neural Network model closely matches the CFD results.

It should be noted that QRSM failed to maintain a good level of accuracy in the CFD validation phase although it demonstrated an outstanding performance for the cases in the Design of Experiment. This raises concerns about overfitting in the training process of the QSRM.

Table 7. Comparison of CFD solutions to the model predictions

Model Name	Model Thrust (N)	Model Torque (Nm)	CFD Thrust (N)	CFD Torque (Nm)	Thrust Error (%)
QRSM	1230.7	135.0	1208	133.3	1.88
SVR	1258.4	135.0	1230	136.8	2.31
ANN	1235.6	135.0	1235	136.0	0.05

Table 8 gives the maximum thrust values of the mode with the optimized variables. When the table is examined, it is seen that the thrust is increased by approximately %7.4 with the artificial neural network regression model.

Table 8. Increase in thrust values with respect to the baseline geometry

Model Name	CFD Thrust (N)	Baseline Thrust (N)	Thrust Increase (%)
QRSM	1208	1150	5.04
SVR	1230	1150	6.96
ANN	1235	1150	7.39

4. Conclusion

In this study, the cubic spline-based twist distribution of the Caradonna-Tung helicopter blade was optimized by adjusting the twist angles at the root, midspan, and tip locations. Additionally, the rate of change of the twist angles at the root and tip was taken into account.

The Box-Behnken Design of Experiment method was employed to define the cases applied for training machine learning algorithms. The optimization was performed using metamodels developed with three different machine learning algorithms: the Quadratic Response Surface Method, Support Vector Regression, and Artificial Neural Network method.

All three models were evaluated based on three different performance metrics. While QRSM demonstrated outstanding performance during training, it failed to maintain the same level of accuracy in the CFD validation phase, raising concerns about overfitting in the training process. On the other hand, ANN regression proved to be the most successful model in this study, with its low error values during evaluation, the optimized results obtained through the optimization process, and a mere 0.05% discrepancy in the CFD validation phase. Furthermore, the ANN identified an optimal case that allowed a significantly higher thrust increase compared to the other models. In this regard, this study demonstrates that the ANN model is far more effective than other methods in regression and optimization tasks.

The maximum thrust force achievable without exceeding the experimental torque value was obtained. The results indicate that optimizing the twist distribution can lead to a significant improvement in thrust.

As a result of this machine learning and optimization study, the thrust generated by the baseline geometry was increased by nearly 7.5% without altering the torque value.

Future studies will focus on evaluating the performance of the metamodels in predicting points, outside the feasible optimization region. Additionally, incorporating other rotor blade parameters beyond twist into the process could be explored to achieve even higher-performance geometries.

Conflicts of Interest

The authors declare that there is no conflict of interest regarding the publication of this paper.

References

Andrés-Pérez, E., González-Juárez, D., Martin-Burgos, M. J., & Carro-Calvo, L. (2019). Constrained Single-Point Aerodynamic Shape Optimization of the DPW-W1 Wing Through Evolutionary Programming and Support Vector Machines (pp. 35–48).

Antony, J. (2014). Design of Experiments for Engineers and Scientists: 2nd Edition (2nd ed.). Elsevier.

Bishop, C. M. (2006). Pattern Recognition and Machine Learning (Information Science and Statistics). In Springer-Verlag Berlin Heidelberg. Springer-Verlag.

Box, G. E. P., & Behnken, D. W. (1960). Some New Three Level Designs for the Study of Quantitative Variables. Technometrics, 2(4), 455–475.

Caradonna, F. X., & Tung, C. (1981). Experimental and analytical studies of a model helicopter rotor in hover.

Cavazzuti, M. (2013). Optimization Methods: From Theory to Design. In Springer-Verlag Berlin Heidelberg (1st ed., Vol. 53, Issue 9). Springer Berlin Heidelberg.

Celi, R. (1999). Recent Applications of Design Optimization to Rotorcraft-A Survey. Journal of Aircraft, 36(1), 176–189.

Conlisk, A. T. (1997). Modern Helicopter Aerodynamics. Annual Review of Fluid Mechanics, 29(1), 515–567.

Costes, M., Renaud, T., & Rodriguez, B. (2012). Rotorcraft simulations: a challenge for CFD. International Journal of Computational Fluid Dynamics, 26(6–8), 383–405.

Ganguli, R. (2004). A Survey of Recent Developments in Rotorcraft Design Optimization. Journal of Aircraft, 41(3), 493–510.

Giunta, A., Narducci, R., Burgee, S., Grossman, B., Mason, W., Watson, L., & Haftka, R. (1995, June 19). Variable-complexity response surface aerodynamic design of an HSCT wing. 13th Applied Aerodynamics Conference.

Glaz, B., Friedmann, P. P., & Liu, L. (2008). Surrogate based optimization of helicopter rotor blades for vibration reduction in forward flight. Structural and Multidisciplinary Optimization, 35(4), 341–363.

Haider, B. A., Sohn, C. H., Won, Y. S., & Koo, Y. M. (2017). Aerodynamically efficient rotor design for hovering agricultural unmanned helicopter. Journal of Applied Fluid Mechanics, 10(5), 1461–1474.

Kaya, M. (2019). A CFD based application of support vector regression to determine the optimum smooth twist for wind turbine blades. Sustainability (Switzerland), 11(16).

Li, J., Du, X., & Martins, J. R. R. A. (2022). Machine learning in aerodynamic shape optimization. Progress in Aerospace Sciences, 134(February), 100849.

Li, J., & Zhang, M. (2021). Data-based approach for wing shape design optimization. Aerospace Science and Technology, 112, 106639.

McVeigh, M. A., & McHugh, F. J. (1984). Influence of Tip Shape, Chord, Blade Number, and Airfoil on Advanced Rotor Performance. Journal of the American Helicopter Society, 29(4), 55–62.

Newman, S. J. (2007). Principles of Helicopter Aerodynamics – Second edition J.G. Leishmann Cambridge University Press, The Edinburgh Building, Shaftesbury Road, Cambridge, CB2 2RU, UK. 2006. 826pp. Illustrated. £65. ISBN 0-521-85860-7. The Aeronautical Journal, 111(1126), 825–826.

Renzoni, P., D'Alascio, A., Kroll, N., Peshkin, D., Hounjet, M. H. L., Boniface, J. C., Vigevano, L., Allen, C. B., Badcock, K., Mottura, L., Schöll, E., & Kokkalis, A. (2000). EROS — a common European Euler code for the analysis of the helicopter rotor flowfield. Progress in Aerospace Sciences, 36(5–6), 437–485.

Sun, G., Sun, Y., & Wang, S. (2015). Artificial neural network based inverse design: Airfoils and wings. Aerospace Science and Technology, 42, 415–428.

Sun, H., & Lee, S. (2005). Response surface approach to aerodynamic optimization design of helicopter rotor blade. International Journal for Numerical Methods in Engineering, 64(1), 125–142.

Vu, N. A., & Lee, J. W. (2015). Aerodynamic design optimization of helicopter rotor blades including airfoil shape for forward flight. Aerospace Science and Technology, 42, 106–117.

Wang, Q., & Zhao, Q. (2020). Rotor blade aerodynamic shape optimization based on high-efficient optimization method. Proceedings of the Institution of Mechanical Engineers, Part G: Journal of Aerospace Engineering, 234(2), 375–387.

You, Y., & Jung, S. N. (2017). Optimum active twist input scenario for performance improvement and vibration reduction of a helicopter rotor. Aerospace Science and Technology, 63, 18–32.

Zhang, X., Xie, F., Ji, T., Zhu, Z., & Zheng, Y. (2021). Multi-fidelity deep neural network surrogate model for aerodynamic shape optimization. Computer Methods in Applied Mechanics and Engineering, 373, 113485.

Cite this article: Ozyilmaz, E.B, Kaya, M. (2025). A Comparative Metamodel Based Shape Optimization Study for Maximizing Thrust of a Helicopter Rotor Blade Under a Torque Constraint. Journal of Aviation, 9(2), 241-248.